Remote sensing of suspended sediment concentration, flow velocity, and lake recharge in the Peace-Athabasca Delta, Canada

Tamlin M. Pavelsky[1] and Laurence C. Smith[2]

[1]   The transport of fine sediment, carried in suspension by water, is central to the hydrology, geomorphology, and ecological functioning of river floodplains and deltas. An extensive new field data set for the Peace-Athabasca Delta (PAD), Canada quantifies robust positive relationships between in situ suspended sediment concentration (SSC) and remotely sensed visible/near-infrared reflectance. These relationships are exploited using SPOT and ASTER satellite images to map suspended sediment concentrations across the PAD for four days in 2006 and 2007, revealing strong variations in water sources and flow patterns, including flow reversals in major distributaries. Near-daily monitoring with 276 MODIS satellite images tracks hydrologic recharge of floodplain lakes, as revealed by episodic infusions of sediment-rich water from the Athabasca River. The timing and magnitude of lake recharge are linked to springtime water level on the Athabasca River, suggesting a system sensitive to changes in river flow regime. Moreover, recharge timing differentiates lakes that are frequently and extensively recharged from those recharged more rarely. Finally, we present a first estimation of river flow velocity based on remotely sensed SSC, though saturation may occur at velocities >0.6 m/s. Viewed collectively, the different remote sensing methodologies presented here suggest strong value for visible/near-infrared remote sensing of suspended sediment to assess hydrologic and sediment transport processes in complex flow environments. Field observations including nephelometric turbidity, specific conductivity, water temperature, Secchi disk depth, suspended sediment concentration, and water level are archived at the Oak Ridge National Laboratory Distributed Active Archive Center for Biogeochemical Dynamics (available at http://daac.ornl.gov//HYDROCLIMATOLOGY/guides/PAD.html).

1. Introduction

[2]   The suspension, transport, and deposition of sediment rank among the most important geomorphic processes in shaping the physical landscape and regulating ecological systems [*Knighton*, 1998]. They are particularly critical in floodplain and deltaic environments, where most landscape features are formed by the movement of sediment and water [*Gomez et al.*, 1995]. Therefore, observation of spatial and temporal patterns in sediment transport is helpful in understanding the formation and function of these environments and how they may respond to natural and anthropogenic perturbations in the future.

[3]   A common measure of sediment transport is suspended sediment concentration (SSC), the mass of sediment entrained within a unit volume of water. A variety of field-based methods have been developed to measure SSC. Most commonly, a water sample is collected in the field and filtered to extract suspended matter. The filtered material is then dried, weighed and divided by the sample volume to obtain SSC concentration (mg/L). Other methods exploit changes in the optical or acoustic properties of water associated with variations in SSC [*Wren et al.*, 2000]. Field-based methods provide accurate, point-based measurements of SSC, but spatial variations are rarely captured and temporal resolution is often limited [*Curran and Novo*, 1988; *Miller and McKee*, 2004].

[4]   Satellite remote sensing offers an alternative option for tracking spatial and temporal variations in SSC. It is especially useful in large, remote or complex hydrologic environments where in situ monitoring is insufficient or impractical. Most techniques for remote sensing of SSC construct empirical relationships between reflectance and in situ measurements collected simultaneously in the field [*Curran and Novo*, 1988; *Schmugge et al.*, 2002]. Sensitivity to SSC variations is generally highest in the red portion of the spectrum (~620–740 nm) [*Schiebe et al.*, 1992], though a combination of several visible and near-infrared bands often produces the most robust SSC-reflectance relationships [*Stumpf and Pennock*, 1989]. Reflectance-SSC regressions are generally highly effective (often $R^2 >$

[1]Department of Geological Sciences, University of North Carolina at Chapel Hill, Chapel Hill, North Carolina, USA.
[2]Department of Geography, University of California, Los Angeles, California, USA.

0.8) and have been successfully used to remotely estimate SSC in a wide variety of fluvial and oceanic environments.

[5] Suspended sediment concentrations normally exhibit a strong statistical relationship with such hydraulic flow parameters as discharge and velocity [*Maidment*, 1993]. In particular, a relationship between flow velocity and SSC has been observed at least since the pioneering work of *Leopold and Maddock* [1953]. Therefore, it would seem possible in principle to infer flow velocities from satellite-derived SSC values, at least in systems where the prime determinant of suspended solids is flow capacity rather than sediment supply.

[6] Rising pressure on water resources, coupled with a poor global monitoring capability, have intensified efforts to remotely measure river hydraulic properties using satellites [*Alsdorf et al.*, 2007a; *Alsdorf and Lettenmaier*, 2003]. Of the three fundamental hydraulic determinants of river discharge (width, depth, and velocity), substantial progress has been made in remote sensing of variations in water level [e.g., *Smith*, 1997; *Kouraev et al.*, 2004; *Coe and Birkett*, 2004; *Frappart et al.*, 2006; *Raclot*, 2006; *Alsdorf et al.*, 2000, 2007b] and width [e.g., *Smith et al.*, 1995, 1996; *Townsend and Foster*, 2002; *Bjerklie et al.*, 2005; *Temimi et al.*, 2005; *Ashmore and Sauks*, 2006; *Brakenridge et al.*, 2005, 2007; *Smith and Pavelsky*, 2008; *Pavelsky and Smith*, 2008b]. However, there are currently few options for remote sensing of flow velocity. Along-track synthetic aperture radar interferometry (ATI) has been used to estimate surface currents in rivers [*Bjerklie et al.*, 2005] and coastal oceans [*Siegmund et al.*, 2004], but the technology is currently unavailable from space and wind significantly contaminates the derived velocity values. The time lag between remotely sensed upstream and downstream width variations can be used to establish a river's average "flow propagation speed" [*Smith and Pavelsky*, 2008] but not instantaneous measurements of velocity.

[7] In complex floodplain and delta environments, the hydrologic recharge of lakes and wetlands is critical to ecological function. However, our capability for observing such recharge remains limited. Remote sensing offers strong promise [e.g., *Smith and Alsdorf*, 1998; *Mertes*, 2000; *Alsdorf*, 2003; *Frazier et al.*, 2003; *Alsdorf et al.*, 2007b; *Pavelsky and Smith*, 2008a] but is often limited by a low temporal sampling rate or requires correlating long time series of satellite images with ground data. Where floodplain lakes are replenished by sediment-rich rivers, however, the presence of high SSC in lakes is a sure indicator of hydrologic recharge from river water. Therefore, using a high temporal resolution sensor (e.g., MODIS), it may be possible to monitor the timing and duration of high-sediment incursions and, thus, lake recharge.

[8] In this study, we examine applications of remote sensing to the study of suspended sediment transport and flow velocity in the Peace-Athabasca Delta (PAD), Canada, a large complex wetland at the confluence of the Peace and Athabasca Rivers with Lake Athabasca. Following a brief review of the published literature on remote sensing of SSC, we describe the PAD study site and our field and remote sensing sampling campaigns. Results include (1) robust relationships between SSCs and remotely sensed reflectance; (2) spatial maps of SSC from four high-resolution ASTER satellite images, based on these relationships;

(3) detection of hydrologic recharge events in floodplain lakes using daily MODIS images; and (4) a first estimation of river flow velocity from remotely sensed reflectance.

2. Remote Sensing of Suspended Sediment Concentration in Freshwater and Estuarine Environments: A Review

[9] Remote sensing of suspended sediment concentration is dependent upon how SSC variations alter the optical properties of the water column. Assessment of SSC and nephelometric turbidity in freshwater and estuarine environments was among the earliest hydrologic applications of satellite remote sensing [e.g., *Ritchie et al.*, 1976; *Holyer*, 1978]. Turbidity, a measure of optical clarity, can be quantified directly using a light turbidimeter, or visually using Secchi disc depth. Because sediment concentration is often the primary control on turbidity, the two quantities are frequently treated similarly with respect to remote sensing [*Ritchie et al.*, 2003]. Methods used to assess SSC and/or turbidity have different variants, but nearly all construct empirical relationships between in situ water quality data and remotely sensed reflectance values. These relationships generally take the form of a linear or exponential regression equation [*Curran and Novo*, 1988; *Schmugge et al.*, 2002; *Topliss et al.*, 1990], though recent work suggests that a neural network approach can improve on these basic statistical relationships [*Keiner and Yah*, 1998; *Wang et al.*, 2008]. In addition, spectral mixture analysis has been successfully used to map SSC [*Mertes et al.*, 1993; *Mertes*, 2002; *Gomez et al.*, 1995; *Matsuhisa and Fukushima*, 2008].

[10] The principal methodological difference among such studies is the choice of spectral band(s) from which to extract reflectance measurements. The simplest approach utilizes reflectance from a single band in the red portion of the spectrum, e.g., Landsat TM band 3 or MODIS band 1 [*Shi and Wang*, 2009; *Miller and McKee*, 2004; *Islam et al.*, 2001; *Hellweger et al.*, 2006; *Nellis et al.*, 1998; *Woodruff et al.*, 1999]. However, laboratory studies suggest robust reflectance-SSC relationships throughout the visible portion of the spectrum [*Novo et al.*, 1991; *Liedeke et al.*, 1995; *Schiebe et al.*, 1992], and many studies combine red reflectance with reflectance in one or more other visible bands in order to increase robustness when sediment color varies [*Wu et al.*, 2007; *Dekker et al.*, 2001; *Han et al.*, 2006; *Tassan*, 1997; *Lathrop et al.*, 1991; *Aranuvachapun and Walling*, 1988; *Lathrop et al.*, 1991].

[11] While the high sensitivity of the visible portion of the spectrum, especially red, to variations in SSC is well documented, portions of the near-infrared spectrum are also sensitive to SSC and have the advantage of being less influenced by bottom reflectance in shallow water environments than do shorter wavelengths [*Tolk et al.*, 2000]. As a result, several studies have successfully utilized near-infrared reflectance alone to assess variations in turbidity or SSC [*Wass et al.*, 1997; *Sterckx et al.*, 2007]. More commonly, however, near infrared reflectance is used in combination with red reflectance [*Doxaran et al.*, 2002, 2003; *Holyer*, 1978; *Ruhl et al.*, 2001; *Wang et al.*, 2008; *Xia*, 1993] or reflectance in multiple visible bands [*Cozar et al.*, 2005; *Ekercin*, 2007; *Fraser*, 1998; *Ritchie and Cooper*,
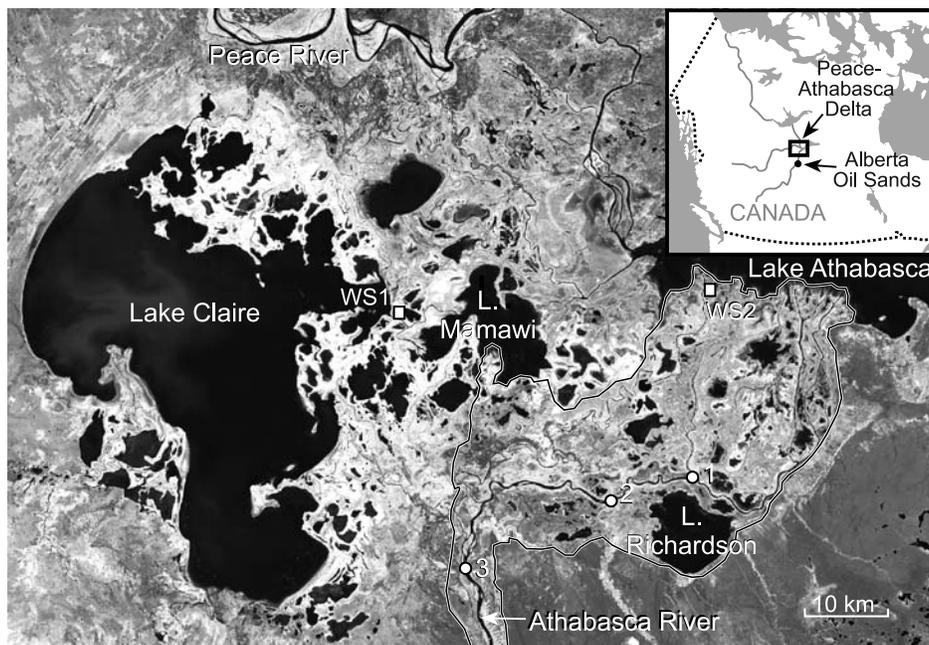
Figure 1. Landsat Band 4 (near infrared) image of the Peace-Athabasca Delta acquired August, 1999. Dark areas are inundated. The black and white line shows the extent of the Athabasca Delta, the principal focus area of this study. Locations of sediment sampling sites in Figure 13 are shown as white circles and weather stations are shown as squares. Inset map shows location of delta within Canada.

1988; *Schiebe et al.*, 1992; *Stumpf and Pennock*, 1989; *Tassan*, 1994; *Topliss et al.*, 1990; *Tripathi et al.*, 1998; *Ritchie and Cooper*, 1991] via a multiple linear regression approach, creation of a ratio-based index, or through the construction of a single metric from multiple bands. In cases where hyperspectral imagery or ground-based spectrometer data are available, variations in the derivative of observed spectra in the 570 to 680 nm and 800 to 930 nm portion of the spectrum have also been effectively utilized to create empirical relationships with SSC [*Chen et al.*, 1992].

[12] All of these approaches result in robust statistical relationships between satellite-derived reflectance and ground-based SSC or turbidity data, with coefficients of determination (r^2) ranging from 0.60 to 0.99. Principle sources of uncertainty in these relationships result from differences in sediment color, grain size, and mineralogy within a study region [*Choubey*, 1998; *Novo et al.*, 1989; *Han and Rundquist*, 1996], from bottom reflectance in shallow areas where suspended sediment concentrations are less than 100 mg/L [*Tolk et al.*, 2000], from contamination by chlorophyll, carotenoids, and other reflective suspended or dissolved material [*Tassan*, 1994; *Quibell*, 1991; *Han*, 1997], and from differences in atmospheric correction techniques [*Stumpf and Pennock*, 1989]. Additionally, in regions with SSC values greater than 250 mg/L some studies have found that reflectance begins to saturate and that the SSC-reflectance relationship becomes logarithmic [*Ritchie and Cooper*, 1988; *Ritchie et al.*, 2003]. *Xia* [1993] suggests that this problem can, in part, be resolved by using a band ratio between a red band such as Landsat TM band 3 and a short-wave infrared band such as TM band 5.

[13] In areas with stratified water masses of different provenance such as river plumes, the depth of a high-sediment water layer can influence reflectance. *Tassan*

[1997] introduces an innovative solution in which separate reflectance-SSC relationships are created using Landsat TM band 2 (green) and band 3 (red). Because the penetration depth of photons in water depends on wavelength, the ratio of sediment concentrations derived using these two relationships can be used to assess the structure of such a stratified water column. Relationships between reflectance and SSC are generally transferable over time for the same location so long as the source of sediment does not substantially vary [*Ritchie et al.*, 2003; *Dekker et al.*, 2002]. Use of a relationship developed in one locale to assess variations in sediment concentration in other areas may be possible in some cases, though such a transfer can be problematic due to differences in sediment quality (e.g., color, size, mineralogy) [*Ritchie and Cooper*, 1991; *Liu et al.*, 2003; *Lathrop*, 1992; *Fraser*, 1998; *Dekker et al.*, 2002; *Ritchie et al.*, 2003].

3. Study Area

[14] Canada's Peace-Athabasca Delta (PAD), a 5200 km^2 freshwater delta at the confluence of the Peace and Athabasca Rivers with Lake Athabasca, ranks among the world's most globally significant boreal wetlands (Figure 1). Because of its high biological diversity, the PAD has been declared a Ramsar Convention Wetland, a UNESCO world heritage site, and is partially protected within Wood Buffalo National Park, Canada's largest park. Other than some exposed bedrock features in the northern sector, the PAD consists of hundreds of interconnected wetlands, shallow lakes (<2 m depth), and active and relict distributary channels. It is typical of most delta ecosystems, which depend largely upon regular recharge of sediment and water. Without such recharge, the grass- and sedge-dominated wetlands and shallow lakes revert to Salix-dominated envi-

Table 1. Water Quality and Hydraulic Flow Parameters Collected in the Peace-Athabasca Delta During 2006 and 2007 Field Seasons

Parameter	Units	Observations
Secchi Depth	cm	560
Turbidity	NTU	541
Water Temperature	°C	541
Specific Conductivity	mS	541
Wind Speed	m/s	515
Wind Direction	–	492
Flow Velocity	m/s	433
Water Depth	m	482
Suspended Sediment Concentration	mg/L	500

ronments that are less biologically productive and less conducive to use by migratory birds [*Prowse and Conly*, 2002; *Toyra and Pietroniro*, 2005; *Timoney*, 2006, 2009].

[15] Under normal flow conditions the Athabasca River, entering from the south, is the major source of sediment and water to the PAD. More rarely, the Peace River also recharges the delta during extreme floods triggered by ice jams [*Beltaos et al.*, 2006; *Leconte et al.*, 2001; *Peters et al.*, 2006]. The last such flood occurred in 1996–1997, ending a 22 year period with no major inflow of Peace River water into the PAD. The hydrology of the PAD has received extensive attention in recent years over concerns about the impact of the Bennett dam on the Peace River [e.g., *Peace-Athabasca Delta Project Group*, 1973; *Prowse and Lalonde*, 1996; *Pietroniro et al.*, 1999; *Wolfe et al.*, 2005; *Peters et al.*, 2006] and water withdrawal for crude oil production in the Alberta Oil Sands development, upstream on the Athabasca River [*Pavelsky and Smith*, 2008a; *Schindler and Donahue*, 2006].

[16] The movement of suspended sediment within the PAD remains largely unstudied despite the critical importance of sedimentary processes to the formation and evolution of the delta. After the end of the last glaciation around 11.8 ka BP, the modern-day PAD was inundated by Lake McConnell, a large proglacial lake that persisted until ~8.3 ka BP [*Smith*, 1994]. Isostatic rebound associated with deglaciation subsequently resulted in the drainage of Lake McConnell and the gradual creation of the PAD in its present form. Today, the delta can be separated into three regions: the Athabasca River Delta, a prograding avulsion belt occupying the southern portion of the delta; the Peace River Delta, a largely relict formation occupying the northern PAD; and a transitional area between the Peace and Athabasca Deltas dominated by several large lakes, including Lake Claire and Lake Mamawi [*Peters et al.*, 2006]. The Athabasca region is the primary focus of this study and its approximate boundaries, together with these three regions, are delineated in Figure 1.

4. Data and Methods

4.1. Field Methods

[17] In situ measurements of water quality, hydraulic variables, and meteorology were collected throughout the study area via boat, helicopter and semipermanent installations during summers 2006 and 2007. Measured water quality variables include nephelometric turbidity, specific conductivity, water temperature, Secchi disk depth (SDD), and suspended sediment concentration (SSC) (Table 1). Measured

hydraulic variables include water depth, flow velocity, and flow direction. In total, one or more of these variables was measured at 102 locations throughout the study area over the course of two summers, yielding a total of 657 data points. Locations were sampled 1 – 25 times, with many revisited 8–15 times over the two year study. The complete data set is archived at the Oak Ridge National Laboratory Distributed Active Archive Center for Biogeochemical Dynamics (available at http://daac.ornl.gov//HYDROCLIMATOLOGY/guides/PAD.html) [*Pavelsky and Smith*, 2009].

[18] Turbidity, conductivity, and temperature were collected using a Eureka Manta® multiprobe. At each sampling point, observations were collected at 2 s intervals, and at least 30 observations were averaged in order to ensure good measurement quality. Two measurements of SDD were collected, one with the disk descending in the water column and the other with the disk ascending, and averaged to provide a single value for SDD. Water surface grab samples were collected from the top of the water column (0 – 30 cm depth) in 250 ml Nalgene® sample bottles, and suspended solids were filtered onto 1.2 μm Millipore cellulose filters using a vacuum-based filtration system. Filters were dried for 1 h at 60°C before and after filtration then weighed on an analytic balance with precision to 0.001 g to determine mass of suspended solids. Filters were then ignited at 550°C for 2 h in a muffle furnace to remove organic components and provide a final value for SSC. All observations of SSC acquired during the summer 2006 and 2007 field seasons are mapped in Figure 2.

[19] Surface flow velocity in rivers and lakes was approximated using a small drogue in combination with a Garmin Geko® handheld GPS and a stopwatch. The drogue was constructed of four rectangular 22 × 28 cm hard plastic panels connected at right angles with L brackets (N.D. Smith, personal communication, 2006). A small float was attached 10 cm above the top of the drogue using parachute cord. To collect surface velocity the drogue was dropped into the water and a GPS point and time were recorded. The drogue was allowed to drift with the current, in most cases for at least 3 min. A second GPS point and time were collected when the drogue was retrieved, and velocity in m/s was calculated using the straight-line distance between the two points and the time the drogue was in the water. Wind speed and direction were collected at two locations within the PAD (Figure 1) on a 15 min time step using Hobo® automated weather stations at 2 m height.

[20] Daily river discharge values for the Athabasca River below Ft. McMurray, approximately 150 km upstream of the PAD, were acquired from Environment Canada (available at http://www.wsc.ec.gc.ca/hydat/H2O/index_e.cfm?cname=main_e.cfm). In addition, water surface elevations were collected at 12 locations throughout the PAD during summers 2006 and 2007 [*Pavelsky and Smith*, 2008a; *Smith and Pavelsky*, 2009]. Water levels were logged every fifteen minutes using submerged Solinst Levelogger® pressure transducers and were corrected for barometric pressure variations using Solinst Barologgers®. Precision of the corrected water levels is ±1 cm. Water level measurements were converted to water surface elevation values using differential GPS-based surveys with accuracy of ±1 to 5 cm. All elevation values presented were leveled to the Canadian Gravimetric Geoid Model 2000 (available at http://www.geod.nrcan.gc.ca/publications/papers/abs26_e.php).
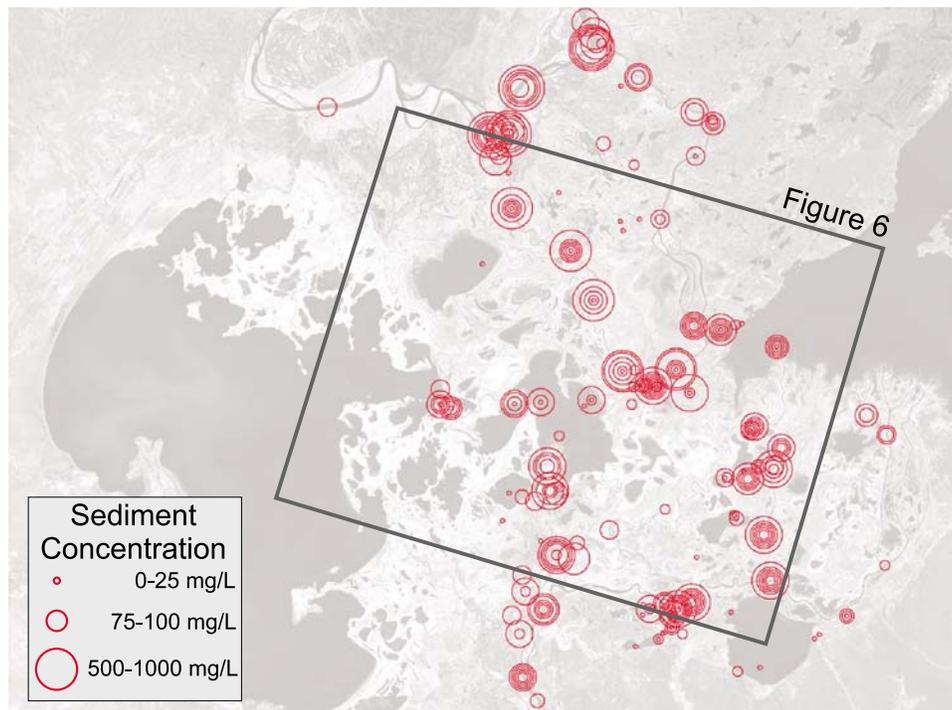
Figure 2. Locations and magnitudes of suspended sediment concentration (SSC) samples collected during summers 2006 and 2007 in the PAD. In total, 500 samples were collected at 93 distinct locations. Highest concentrations are on the Peace and Athabasca Rivers, with generally lower concentrations in lakes and channels within the PAD.

4.2. Remote Sensing Methods

[21] To assess detailed spatial patterns in SSC across the PAD, four high-resolution satellite scenes (two from SPOT, two from ASTER) were acquired during summers 2006 and 2007 (Table 2). All scenes were projected into UTM Zone 12N/WGS 84 and radiometrically and geometrically corrected to account for differences in sun and sensor angles as well as atmospheric conditions. Empirical relationships between the natural logarithm of SSC and red reflectance (band 2 for both sensors) as well as total reflectance (the sum of band 1, 2, and 3 reflectance values) were created for three high-resolution images (1 SPOT, 2 ASTER) coinciding with collection of in situ SSC data. Past studies suggest that reflectance values from one sensor acquired on multiple dates can be successfully combined without biasing the SSC-reflectance relationship [*Miller and McKee*, 2004; *Cozar et al.*, 2005; *Fraser*, 1998]. As a result, we combine data points from the two ASTER images in a single regression analysis. Only those SSC data collected within 48 h of scene acquisition were used in constructing these relationships.

[22] In order to ensure robust SSC-reflectance regressions, we test regression assumptions in three ways. Cook's distance (D_i) is used to measure the statistical influence of each data point by calculating the impact of its removal from the regression [*Cook*, 1977]. A value of $D_i > 1.0$ indicates either a point with high leverage or an outlier. We also include the Breusch-Pagan Test, in which statistically significant ($p < 0.05$) correlation between square residuals and the independent variable (reflectance, in this case) indicates heteroskedasticity [*Breusch and Pagan*, 1979]. Finally, we create

normal probability plots of residuals, in which a high linear correlation between residuals and their z statistics indicate that the residuals are normally distributed [*McPherson*, 2001]. Rather than printing the plots here, we simply provide the correlation coefficients. Values close to 1.0 confirm normal distribution of residuals.

[23] In the six largest lakes within the PAD (including Lake Claire, Lake Mamawi, Lake Athabasca, and Lake Richardson, Figure 1), reflectance remains chronically high throughout the open water season even when measured SSC does not. This persistently high reflectance remains pervasive across all visible and near-infrared ASTER, SPOT and MODIS bands and for all dates, though the spatial extent of water exhibiting the anomalously high reflectance varies over times. The source of this elevated reflectance remains unknown, but appears related to high algal productivity in the largest lakes only. The spatial distribution of chlorophyll *a* concentration from the MODIS chlorophyll product [*Pinkerton et al.*, 2005] closely matches that of anomalously

Table 2. Number of Scenes, Dates, and Spectral Bands From SPOT, ASTER, and MODIS Sensors Used in This Study

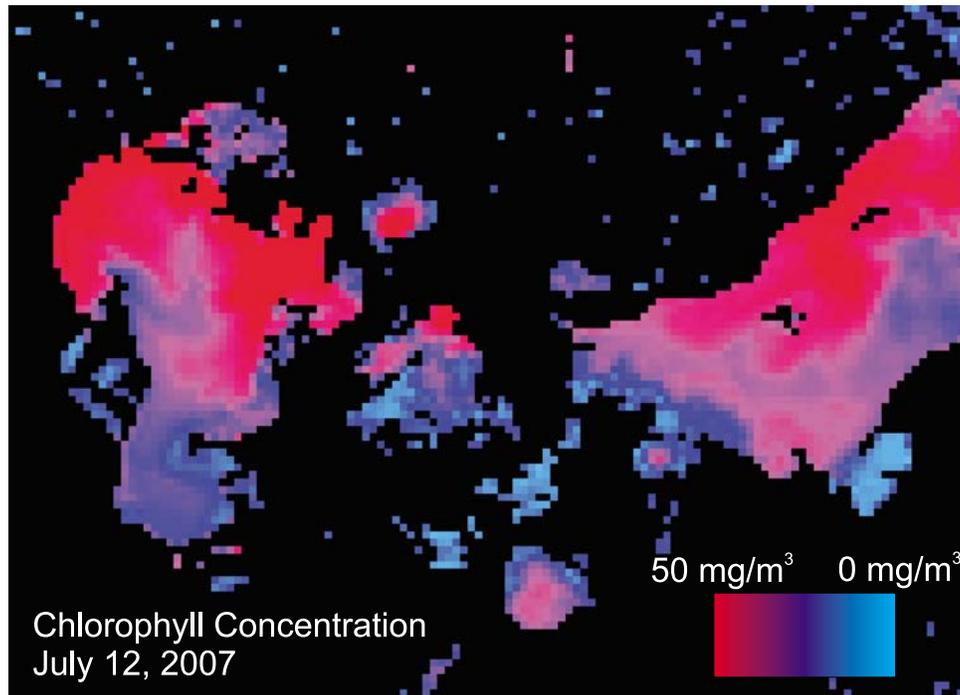| Sensor	Scenes	Dates	Wavelengths
ASTER	2	July 19, 2006 July 13, 2007	band 1 (520–600 nm) band 2 (630–690 nm) band 3 (760–860 nm)
SPOT	2	June 16, 2006 June 14, 2007	band 1 (500–590 nm) band 2 (610–680 nm) band 3 (790–890 nm)
MODIS	276	May 1–Sept. 15, 2006 and 2007	band 1 (620–670 nm) band 2 (841–876 nm)

Figure 3. 1 km MODIS chlorophyll product showing high chlorophyll values in red and low values in blue. High chlorophyll values are likely related to strong algal productivity. Spatial patterns of high chlorophyll match areas in which SSC-reflectance relationships fail due to anomalously high reflectance.

high reflectance, suggesting a link between biological activity and reflectance (Figure 3). These six largest lakes have therefore been excluded from our analysis.

[24] Daily 250 m resolution MODIS Level 2G Aqua and Terra scenes (MOD09QKM and MYD09QKM) were acquired between May 1 and September 15 in 2006 and 2007. All MODIS Level 2G scenes are radiometrically and geometrically corrected to account for differences in sun and sensor angle and variations in atmospheric conditions. These corrections, including those for aerosols, thin cirrus clouds, and adjacency effects associated with land cover variations provide image-to-image consistency in reflectance values and are thus essential to our analysis [*Justice et al.*, 2002]. All scenes were projected into UTM zone 12N/WGS 84. A binary metric to differentiate high- and low-sediment water (M) was created by thresholding the difference between MODIS band 2 (near infrared, 841–876 nm) and band 1 (red, 620–670 nm) reflectance at a value of 0.01:

$$M = \begin{cases} 0 \text{ if } b2 - b1 < 0.01 \\ \\ 1 \text{ if } b2 - b1 \geq 0.01 \end{cases}$$

Images with cloud contamination were eliminated using a simple threshold in band 2. Aside from the six large lakes with anomalously high reflectance discussed above, this threshold is met only for water with high SSC. This allows the metric to be used to capture hydrologic recharge events (in which floodplain lakes are replenished by sediment-laden water from the Athabasca River), in a manner similar to that used by *Mertes* [2000] on the Amazon floodplain,

Shi and Wang [2009] in the Mississippi River Delta, and *Teodoro et al.* [2008] in the Douro River estuary. The volume of Athabasca water entering the floodplain lake can be roughly estimated by dividing the number of high-sediment pixels by the total number of water pixels on a given day using the formula:

$$\text{SAI} = S/A$$

Where S is area of high sediment water in a lake ($M = 1$) and A is total lake area, and SAI is the Sediment Area Index. SAI is useful because it tracks the extent of the sediment-laden plume entering a lake, which (together with its concentration) is proportional to the total suspended sediment transport into the lake basin.

5. Results

5.1. Establishing SSC-Reflectance Relationships

[25] Comparisons of in situ suspended sediment concentrations with turbidity and Secchi dish depth measurements suggest that, as in many freshwater systems, SSC is the primary control on the optical properties of PAD surface waters. Values of SSC collected throughout the PAD over two summers range from nearly clear (∼0 mg/L) in some closed lakes and distributaries to ∼1000 mg/L in the Peace River during high flow (Figure 2). The measured SSCs strongly control water column turbidity and SDD as evidenced by a high correlation (R^2 = 0.88, 0.79 respectively) between the natural logarithm of SSC and both variables (Figures 4a and 4b).
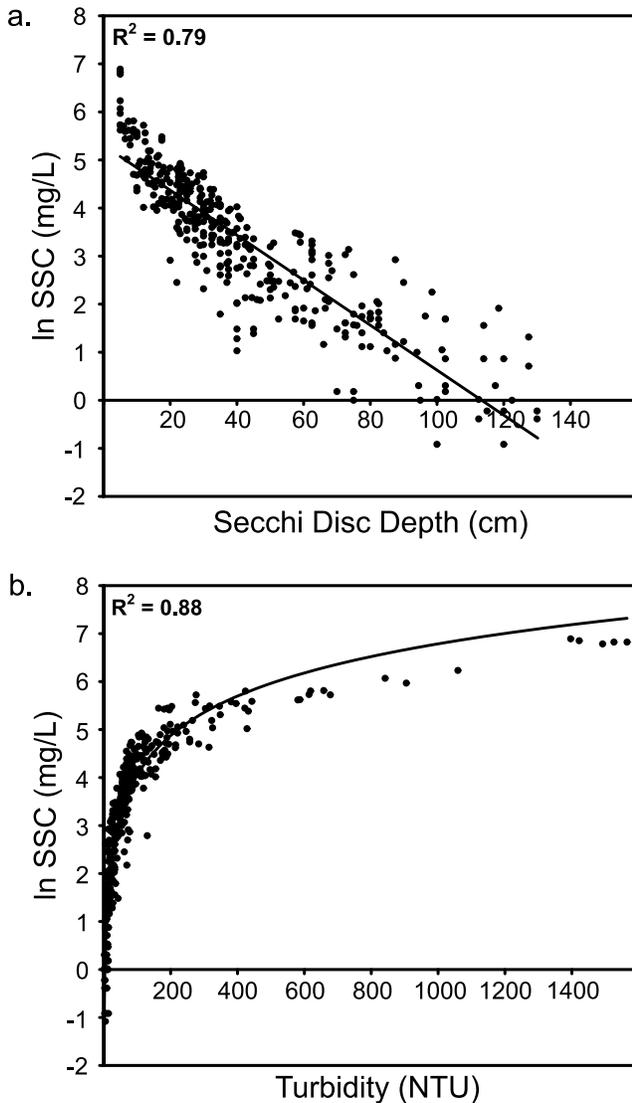
Figure 4. Scatterplots of the natural logarithm (ln) of SSC and (a) Secchi disc depth (n = 434) and (b) nephelometric turbidity (n = 425) using all available data collected in the PAD during summers 2006 and 2007. Robust relationships in both cases suggest that suspended sediment exerts a significant control on the optical properties of the water column.

[26] Strong positive relationships are also found between SSC and remotely sensed red reflectance (R^2 = 0.82, 0.78) and total reflectance (R^2 = 0.89, 0.79) in the SPOT and ASTER scenes for which field data are available (Figure 5). Maximum values of Cook's distance (D_i) are substantially less than 1.0 for all regressions (Table 3), suggesting an absence of outliers or other high-leverage points. High correlation coefficients computed from normal probability plots of residuals (r > 0.98 in all cases) indicate that residuals are normally distributed in all cases. Breusch-Pagan statistics suggest that heteroskedasticity may be present only in the ASTER band 2 regression, likely due to a cluster of low residual data points with high SSCs. As the degree of heteroskedasticity is limited and lacks a physical explanation, we suggest that all four regressions meet assumptions for linear regression analysis.

[27] For both SPOT and ASTER, highest coefficients of determination are associated with total reflectance. This result supports *Schiebe et al.* [1992], who suggest that SSC-reflectance relationships are most robust when multiple spectral bands are used in combination rather than simply red reflectance. It is unsurprising that regression equations created using SPOT and ASTER reflectances differ somewhat, as the wavelengths of the three bands utilized here, while similar, are not identical (Table 2). Regardless of these differences, reflectance values from both sensors exhibit strongly positive linear relationships with the natural log of SSC, allowing reflectance values throughout each image to be exploited to estimate suspended sediment concentrations throughout the PAD on the day each satellite image was acquired.

[28] In order to assess differences in SSC-reflectance relationships among different source regions, we divide the data points in Figure 5 into three regions: the Peace River, Athabasca River, and central PAD. While sample sizes and spread are insufficient to compute reliable statistics, visual examination of Figure 5 suggests that in each regression, points from all regions follow the overall regression line. This is particularly true for the two total reflectance plots, in which variations in sediment color are likely less important than in the plots of red (band 2) reflectance.

5.2. Mapping Suspended Sediment Concentrations in the PAD

[29] The linear relationship between SSC and SPOT total reflectance shown in Figure 5a was used to create the first known maps of suspended sediment concentration in the PAD (Figure 6). *Fraser* [1998] suggests that SSC-reflectance relationships created using SPOT imagery are transferable from scene to scene, and we use the relationship established in Figure 5 (June 14, 2007) to map SSC using SPOT images from June 2006 (Figure 6a) and 2007 (Figure 6b).

[30] In both maps, rivers have generally higher suspended sediment concentrations than do lakes, though this pattern is more pronounced in 2007 than 2006. Overall, June 2007 SSCs are much higher than in June 2006. These elevated SSCs are associated with a known high-water event in the Peace and Athabasca Rivers that resulted in substantial changes in flow direction within the PAD [*Pavelsky and Smith*, 2008a]. Arrows in Figure 6a show the normal direction of flow for major PAD channels, whereas arrows in Figure 6b show the direction of flow recorded on the ground during this unusual high-water event as measured in situ using a drogue (Section 4.1). Major changes include flow reversals on two channels connecting the Peace River with the central portion of the PAD, as well as reversed flows to at least 5 floodplain lakes in the southern PAD. Plumes of high-sediment water are observed near the outlet channels of several of these lakes in Figure 6b, indicating inflow of water from the Athabasca River. In both maps SSC remains constant or decreases downstream, suggesting little resuspension of sediment stored within the PAD, at least during the times these two satellite images were acquired. Maps of sediment concentration were also successfully created using ASTER scenes from July 19, 2006 and July 13, 2007 but are not shown here. Discharge in the Peace and Athabasca Rivers is lower in July than in June, resulting in
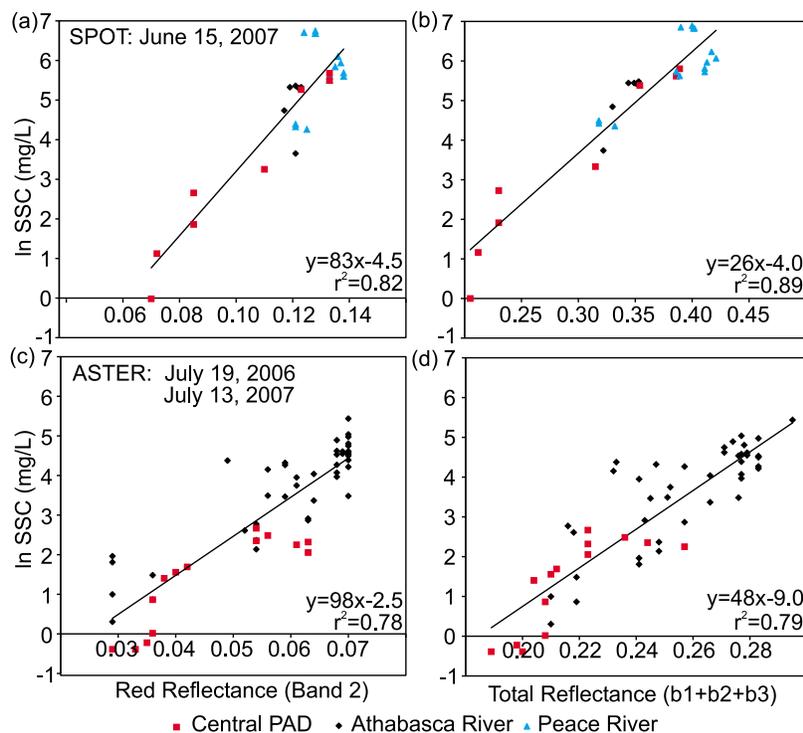
Figure 5. Scatterplots showing the natural logarithm (ln) of in situ SSC measurements and red reflectance (band 2) and total reflectance (band 1 + band 2 + band 3) from one high resolution SPOT image acquired on June 15, 2007 and two ASTER images acquired on July 19, 2006 and July 13, 2007. In each case, the use of total reflectance rather than red reflectance results in a stronger statistical correlation indicated by the higher r^2. Points are colored according to region. In the case of total reflectance, results suggest that mean divergence from the overall regression line does not differ by region.

lower SSCs, but the spatial distributions of SSCs on these ASTER acquisition dates are otherwise similar to those in Figure 6a.

5.3. Remote Sensing of Hydrologic Recharge to Floodplain Lakes

[31] High-resolution maps such as those in Figure 6 provide spatially rich information on patterns of SSC for a particular day, yet they remain problematic from the perspective of monitoring sediment transport and deposition processes continuously due to their low temporal resolution [*Ritchie et al.*, 2003]. In contrast, daily MODIS images have insufficiently fine spatial resolution (250 m) to track suspended sediment concentrations in river channels within the PAD but can detect SSC variations in floodplain lakes with a high temporal sampling rate.

[32] The capture of episodic lake recharge events is illustrated with three MODIS images in Figure 7 (May 18, June 13, and September 7, 2007; band 2). Red tones on each image identify those areas where $M = 1$ (Section 4.2), revealing inflows of sediment-rich Athabasca River water. While high wind events could resuspend bottom sediments in shallow lakes, low correlation between wind speed and lake recharge (r = 0.06) suggests that wind contamination is unlikely here. The previously described large lakes with chronically high reflectance (section 4.2) are masked out in gray. High flows in the Athabasca River (discharge = 3,170 m³/s, May 18, 2007) triggered hydrologic recharge of at least 24 lakes in the southern PAD, as revealed by the

arrival of high-SSC water in the lakes (Figure 7a). Seven of these lakes also received Athabasca River water during a second high water event (discharge = 1,640 m³/s) in mid-June (Figure 7b); and 17 lakes did not. By September (Figure 7c), all floodplain lakes were free of high-SSC water, as Athabasca River discharge had dropped substantially (discharge = 631 m³/s on September 7, 2007).

[33] Figure 8 presents time series of MODIS-derived sediment area index (SAI) for six representative floodplain lakes from the southern, Athabasca-dominated portion of the PAD, plotted from early May through mid-September, 2007. The locations of these six lakes are indicated by numerals in Figure 7a. Discharge in the Athabasca River (downstream of the Alberta Oil Sands, Figure 1) is shown in gray. SAI values in some lakes, especially Lakes 1 and 4, closely track water levels on the Athabasca, suggesting a strong relationship between river stage and hydrologic/

Table 3. Regression Diagnostics for Scatterplots in Figure 5[a]

	Max D_i	B-P r	NPPR r
ASTER Band 2	0.22	0.07	**0.98**
ASTER Total	0.09	0.21	**0.98**
SPOT Band 2	0.33	0.25	**0.99**
SPOT Total	0.25	**0.29**	**0.98**

[a]Includes the maximum value of Cook's distance (D_i), the Breusch-Pagan test statistic (B-P r) and the correlation coefficient from a normal probability plot of residuals (NPPR r). Bold text indicates statistical significance at the $p = 0.05$ level.
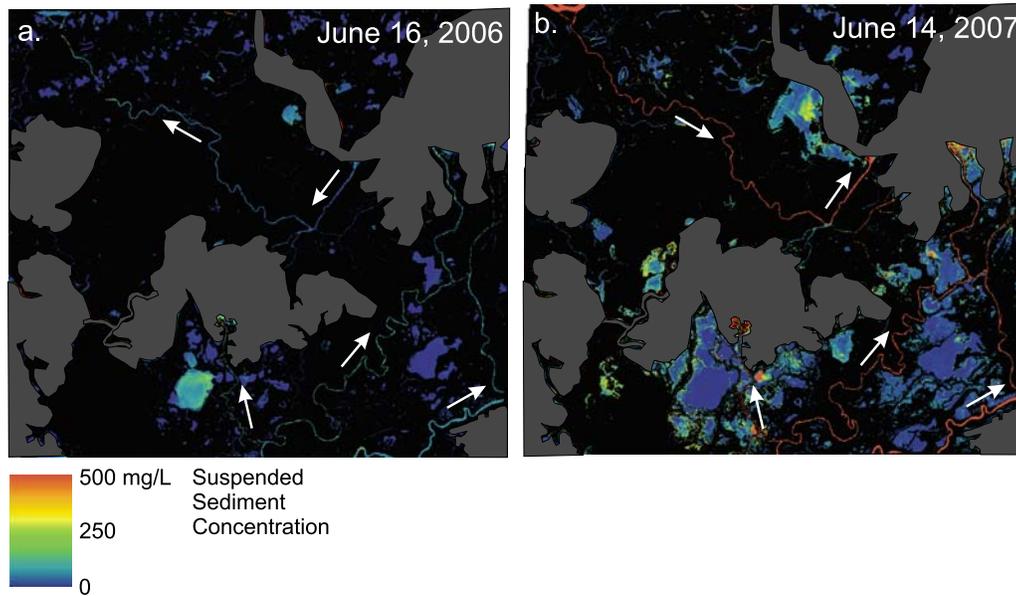
Figure 6. The first known maps of suspended sediment concentration (SSC) for the central portion of the PAD, derived using the SPOT–total reflectance regression equation from Figure 5. Highest concentrations are in red, lowest in blue. Lakes influenced by anomalously high reflectance are masked. Arrows in white show the flow direction under (a) normal conditions and (b) during a high water event coinciding with the collection of the image. Note the reversals of flow direction on two of the major channels, showing the transport of Peace River water into the central portion of the PAD. High-sediment plumes are visible in several lakes in the central and southern PAD in Figure 6b, indicating inflow and recharge from Athabasca River water.

sedimentary recharge. Lakes 3 and 5 have generally high SAI values following the spring flood on the Athabasca but mirror its fluctuations during the open water season less closely. Lake 2 SAI is above zero only in early May, suggesting that water and sediment recharge to this lake occurs only during the spring freshet. Lake 6, one of the large, chronically high-reflectance lakes described earlier, is included here to demonstrate the impact of persistent, anomalously high reflectance on SAI values. Full time series tracking the number of lakes in the Athabasca Delta where $M = 1$ are shown for 2006 (Figure 9a) and 2007 (Figure 9b). In each year, lake recharge is associated most strongly with the period during and immediately following the spring flood, while a lesser number of lakes are replenished by high water events later in the season. The lag between discharge and lake recharge visible in Figure 9 is expected, since the discharge gauge is located some 150 km upstream of the delta.

5.4. Remote Sensing of Flow Velocity

[34] The well-known relationship between at-a-station flow velocity and suspended sediment concentration [e.g., *Leopold and Maddock*, 1953], implies that it may be possible to estimate surface velocity, at least qualitatively, from remotely sensed SSC. Figure 10 shows two velocity-reflectance curves constructed using field-measured velocity data from 30 sampling sites throughout the study area and total reflectance from ASTER scenes collected July 19, 2006 and July 13, 2007. On both days, a robust positive relationship between velocity and reflectance is evident ($R^2 = 0.83$ and 0.84, respectively). However, the regression form is linear in the 2006 ASTER image and exponential in

the 2007 ASTER image. The reason for this difference is unclear, but may indicate temporal hysteresis in the relationship between SSC and river discharge [*Leopold and Maddock*, 1953]. In addition, temporal variations in the size of suspended sediments likely affect SSC-discharge relationships, and resuspension of sediment may vary with discharge and depth.

[35] Maximum D_i values from the two regressions were 0.15 and 0.63, respectively, indicating a lack of outliers or other high-leverage data points. Results from a Breusch-Pagan Test ($r = 0.21$, $p = 0.24$) and normal probability plot of residuals ($r = 0.98$) indicate robustness in the 2006 regression. Given the strong nonlinearity in the 2007 regression, it is unsurprising that the Breusch-Pagan Test shows heteroskedasticity ($r = 0.56$, $p < 0.01$), though the residuals remain normally distributed ($r = 0.98$). We believe that heteroskedasticity results from saturation in the velocity-reflectance relationships at velocities greater than ~0.6 m/s. As such, we consider predicted velocity values above this threshold to be nonrobust.

[36] Despite the presence of heteroskedasticity in the 2007 data, we believe that the regression lines shown in Figures 10a and 10b represents the data sufficiently well that maps of surface flow velocity can be made for the associated image, at least for velocities <0.6 m/s. Figure 11 shows flow velocities for a portion of the southern PAD constructed using the July 2007 ASTER image and rating curve. As anticipated, velocities are highest (red) on the Athabasca River and its distributaries and lowest (blue) in lakes. Because the relationship on which the map is based is exponential in nature, velocity values saturate above approximately 0.6 m/s. As such, it is difficult to discern
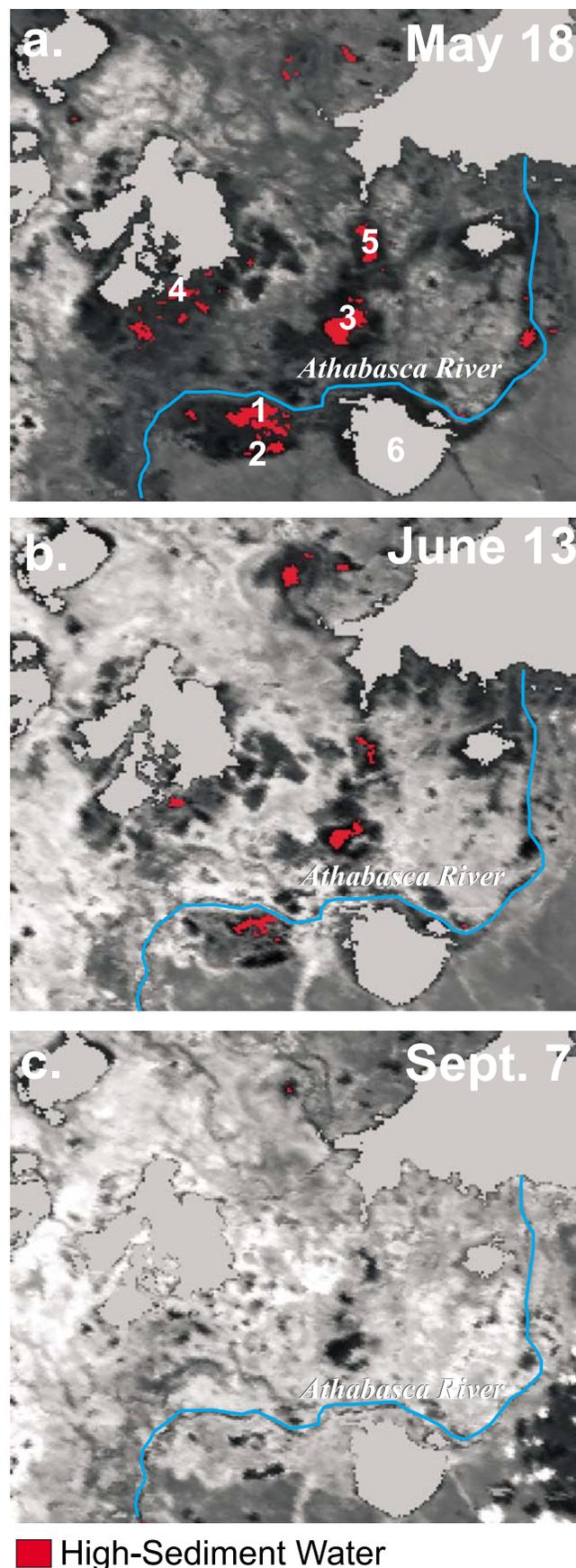
differences in flow velocity on the main stem of the Athabasca River, where velocities are generally close to 1.0 m/s. However, on the Embarras River (a distributary of the Athabasca, shown within a white box in Figure 11), flow velocities are seen to decrease downriver. Ground validation of this decrease is shown in Figure 12, which compares a profile of remotely sensed SSC (July 13, 2007) with in situ measurements of velocity and SSC collected on June 25, 2007. Despite being acquired 18 days apart, the field and satellite SSC data show general agreement. Furthermore, all three data sets indicate a downstream slowing of flow velocity in the Embarras River. This downstream decline in visible/near-infrared reflectance is found in all SPOT and ASTER images included in this study (Table 2).

[37] The question of whether velocity-reflectance rating curves are transferable from image to image remains open. The substantial difference between the two rating curves in Figure 10 suggests that transfer may not be possible. However, statistically significant ($p < 0.01$) relationships between at-a-station velocity and turbidity at three points on the Athabasca River (Figure 13) do suggest that temporal relationships between velocity and SSC can be exploited. Because available data for each location includes outliers with substantial statistical influence, the Pearson's correlation coefficient is an inappropriate measure of covariance. Instead we use Spearman's ρ, a nonparametric test of correlation, which is not influenced by outliers [*Spearman*, 1904]. Further studies are necessary to address image-to-image consistency in velocity-reflectance relationships and collect sufficient in situ data to create robust at-a-station regressions between turbidity and velocity. At a minimum, it appears that relative variations in flow velocity can be identified between different areas of the PAD, at least qualitatively and within the same satellite image.

6. Discussion and Conclusions

[38] There are three principal conclusions to be drawn from this analysis. The first is that robust statistical relationships can be constructed between SSC and remotely sensed reflectance in the complex fluvial environment of the PAD. Unlike previous studies using remote sensing to examine SSCs in river and wetland environments [e.g., *Cozar et al.*, 2005; *Han et al.*, 2006; *Mertes et al.*, 1993; *Wass et al.*, 1997], the PAD receives water from at least three major sources (the Peace and Athabasca Rivers, and also Lake Athabasca), each of which has different source regions for sediment, unique ecological influences, and diverse human impacts. Nonetheless, SSC-reflectance relationships for the PAD are as robust as in many less hydrologically complex regions, especially when multiple visible and near-infrared

Figure 7. Time series of MODIS images can be used to identify episodes of lake recharge with sediment-rich river water. Representative MODIS band 2 images of the PAD are shown for three dates in 2007. Regions in which $M = 1$, which indicates the presence of high-sediment river water, are shown in red. Lakes influenced by anomalously high reflectance (see section 4.2) are masked. Areas of high-sediment water are most pervasive during (a and b) high-water events early in the year and disappear during (c) low-water conditions in September.
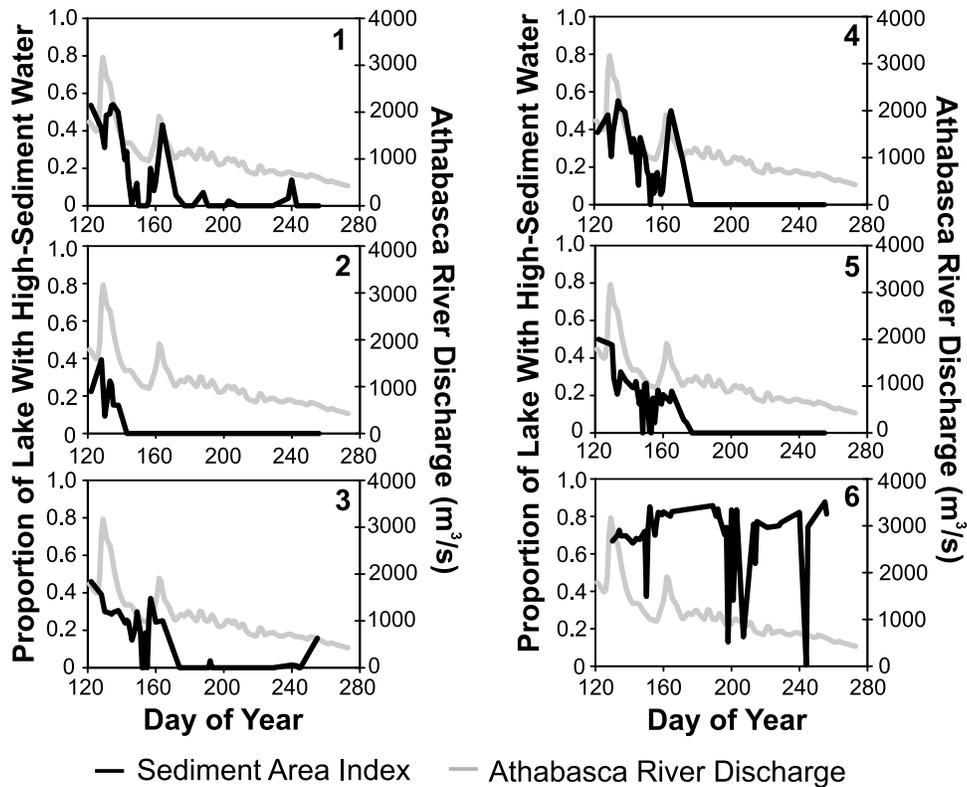
Figure 8. Black lines show time series of SAI derived from summer 2007 MODIS images for six lakes in the southern portion of the PAD. Time series of discharge on the Athabasca River below Ft. McMurray are shown in gray. Locations of lakes are shown in Figure 7a. Sediment recharge of Lakes 1 and 4 closely follows discharge on the Athabasca, while recharge of Lake 2 occurs only during the spring flood. Pervasively high SAI in Lake 6 is the result of anomalously high reflectance values and does not reflect actual sediment recharge.

bands are utilized rather than a single red band. This finding confirms past research using reflectance from multiple spectral bands in other freshwater and estuarine environments [*Schmugge et al.*, 2002; *Ritchie et al.*, 2003]. Like most previous remote sensing studies of SSC we principally focus on only one hydrologic system, and the transferability of regressions developed here to other environments remains unknown. Still, strong similarities in SSC–total reflectance relationships regardless of sediment source region (Figure 5) suggest that future research may allow the extension of such regressions to the regional scale.

[39] However, it is important to note that robust, useful SSC-reflectance relationships were produced only by eliminating 6 large lakes with anomalously high reflectance values from consideration. The cause of their chronic high reflectance values remains unknown, but may result from high algal productivity. The shifting spatial pattern of high reflectance in these lakes clearly mimics those of high chlorophyll *a* concentration (Figure 3). However, chlorophyll *a* alone should not account for high reflectance at all visible and near-infrared wavelengths as it usually has little influence on red reflectance. Therefore, we suggest that a combination of chlorophyll and other biogenic compounds are a likely cause of persistently high reflectance. Future collection of in situ chlorophyll, biogenic silica, and dissolved oxygen data sets in the PAD are needed to confirm or disprove this hypothesis.

[40] The second principal conclusion of this study is that it is possible to detect the episodic recharge of PAD floodplain lakes with river water, using daily MODIS data to identify when sediment-rich plumes enter the lakes. In complex wetland environments like the PAD numerous ecological and biogeochemical processes depend on such infusions, which cannot necessarily be detected from multi-temporal maps of water surface area, e.g., from synthetic aperture radar (SAR) data [*Smith and Alsdorf*, 1998]. While it is possible that floodplain lakes in the PAD may be recharged from other sources without receiving high-sediment river water from the Athabasca River, recharge and hydrologic connectivity are a certainty when high-SSC river water is observed in a lake. As such, time series of SAI can be used to differentiate lakes that are frequently and extensively recharged (such as Lakes 1 and 4 from Figure 8) from those which are recharged more rarely, in some cases only during the spring flood (e.g., Lake 2).

[41] The close agreement between the number of Athabasca Delta lakes recharged and Athabasca River discharge (Figure 9) suggests that lake recharge is principally controlled by variations in river flow. Moreover, the greater number of lakes recharged during peak spring flow in 2007 (high spring flood) compared to 2006 (minimal spring flood) suggests that replenishment of water and sediment is highly dependent on Athabasca River flow during this crucial period. Like *Pavelsky and Smith* [2008a], we find
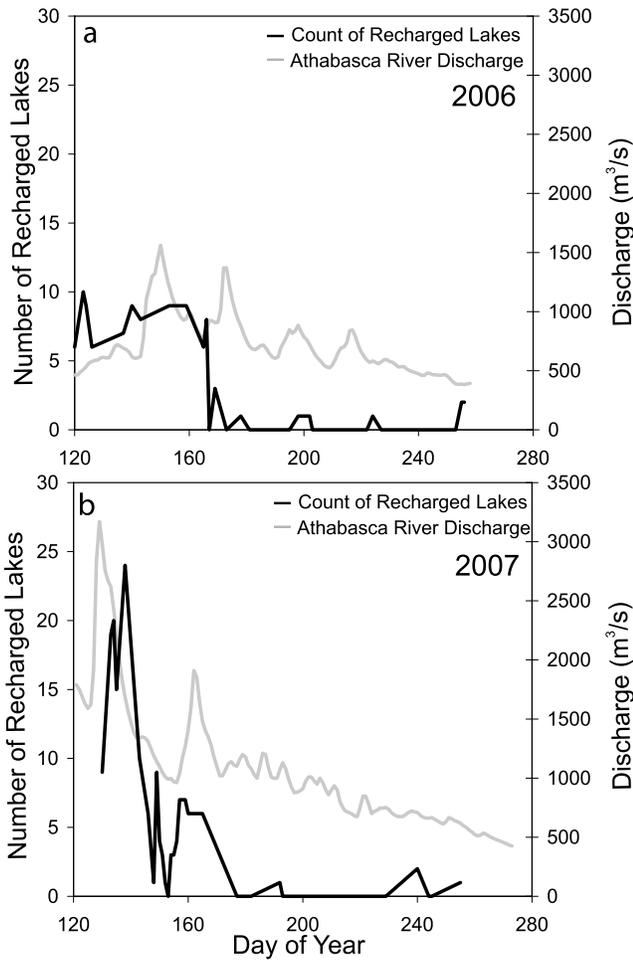
Figure 9. Black lines show time series of the number of study area lakes receiving high sediment water ($M = 1$) throughout summers (a) 2006 and (b) 2007. Gray lines show Athabasca River discharge over the same periods. Lake counts were obtained from a series of MODIS images like those shown in Figure 7. In each year principal lake recharge occurs during the spring flood, while later high water events affect only a limited number of lakes.

coupling of lake recharge and river flow indicates a system that may be highly sensitive to long-term changes in flow on the Athabasca River, especially during the spring flood.

[42] Prior to this study, assessing the frequency of recharge events has been problematic due to the difficulty of obtaining field-based data in such environments and a lack of satellite data with daily temporal resolution and adequate spatial resolution [*Pavelsky and Smith*, 2008a; *Alsdorf et al.*, 2007b]. Even MODIS data are only useful for monitoring lakes $>\sim25$ ha, and are too coarse for the study of river channels. Extension of the SAI metric to track interannual variations in water and sediment recharge across the PAD would allow assessment of vulnerability to future changes in the Athabasca River flow regime. Mean annual flow in the Athabasca has decreased by approximately 20% since
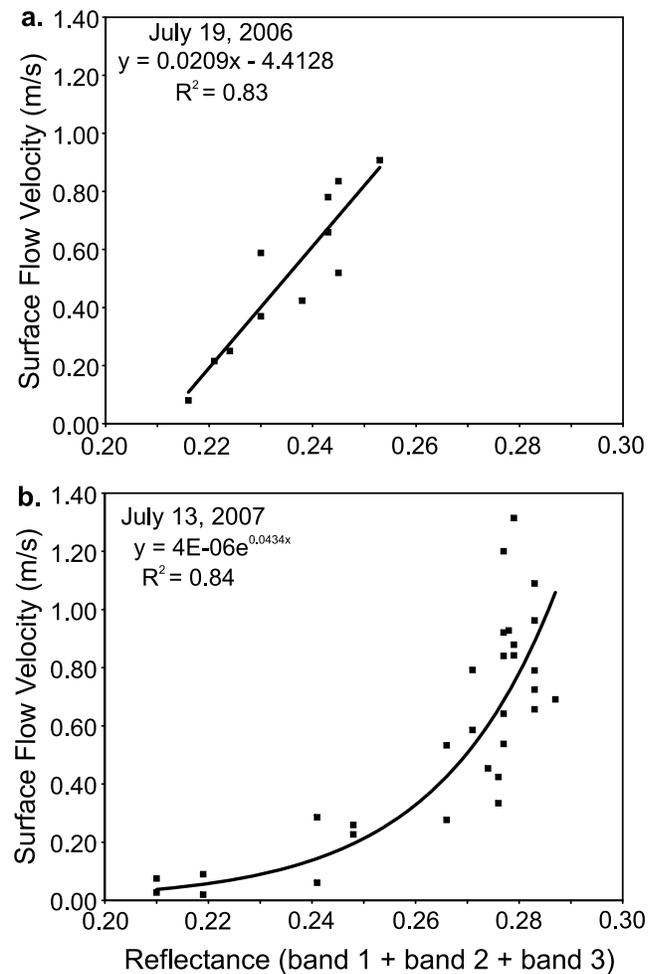

Figure 10. Scatterplots showing regression relationships between surface flow velocity at points within the Athabasca River Delta and total reflectance (band 1 + band 2 + band 3) for two ASTER images. In situ velocity data were collected within 0–48 h of satellite image acquisition. Both plots show strong agreement between velocity and reflectance, suggesting that spatial variations in velocity within an image can be remotely sensed. The difference in regression equation form ((a) linear, (b) exponential) may be related to temporal hysteresis in the relationship between SSC and river discharge.
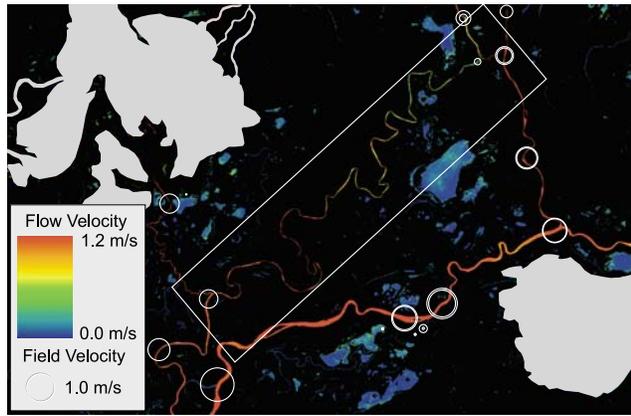
that most lakes are recharged only during the spring flood. However, we also find that a limited number are recharged during the secondary high-water event in mid-June, suggesting that some portions of the PAD may be sensitive to high water events other than the spring freshet. This finding appears somewhat at odds with the results of *Pavelsky and Smith* [2008a], which found little sensitivity of PAD inundation area to summer high-water events. Closer examination, however, reveals that lakes shown here to be recharged during summer high water events match closely with the few areas of the PAD that appear sensitive to Athabasca River flows in that study. The conclusion of both studies, then, must be that delta-wide recharge is associated only with the spring flood, while a more limited subset of lakes and wetlands can be replenished through summertime high-water events. The current findings also support *Wolfe et al.* [2007], who utilize varying isotopic signatures of lake water throughout the PAD to track sources of recharge. Such close

Figure 11. The first known map of surface flow velocities created using an empirical velocity-reflectance relationship. Velocities were derived from ASTER image acquired July 13, 2007 using regression equation shown in Figure 10b. The velocity relationship was calibrated using 30 in situ velocity measurements (shown as white circles) collected within 0−48 h of the satellite image acquisition. Highest velocities are in red, lowest in blue. The Embarras River (white box) shows decreasing downstream velocity and is shown in profile in Figure 12.

Figure 12. Profile of SSC values shown in black for the boxed portion of the Embarras River in Figure 11. In situ SSC measurements obtained June 25 are shown as black squares, and velocity measurements are shown as gray squares. In all three data sets, SSC or velocity decreases with distance downstream. This pattern matches the pattern of derived velocity values on the Embarras in Figure 11.

1958, largely in response to diminished contribution from snowpack and glaciers in the Canadian Rockies, and this trend is expected to continue in response to anthropogenic climate change [*Schindler and Donahue*, 2006]. In addition, increased petroleum production in the Alberta Oil Sands will require substantial diversions of water from the Athabasca over the next decade [*Griffiths et al.*, 2006]. While near-term withdrawals are unlikely to significantly impact hydrologic recharge and sediment transport in the PAD during the open water season, further diversions, when combined with the effects of climate change, may result in substantial impacts [*Pavelsky and Smith*, 2008a]. The methodology presented here may help identify and monitor those areas of the PAD most vulnerable to reduced inputs of water and sediment from the Athabasca River.

[43] The third conclusion of this study is that it appears possible to extract variations in surface flow velocity from remotely sensed imagery by exploiting the positive relationship between velocity and SSC. Substantial progress has been made in recent years in remote sensing of river discharge, yet methods for remote estimation of flow velocity (a central component of discharge calculation) remain in virtual infancy [*Siegmund et al.*, 2004; *Bjerklie et al.*, 2005; *Alsdorf et al.*, 2007a]. The method presented here is entirely different from previous methods utilizing along-track SAR interferometry (ATI) and avoids the main problems of that technique, notably the lack of available satellites and contamination by wind. It allows for mapping of velocities with moderate spatial resolution, permits at least a qualitative if not quantitative assessment, and a relationship between SSC and velocity may exist over time as well as space. Unlike ATI, however, it does not directly measure velocity but a proxy for it (SSC) that is also influenced by other factors like upstream supply and local sources and sinks of sediment. Moreover, the form of the
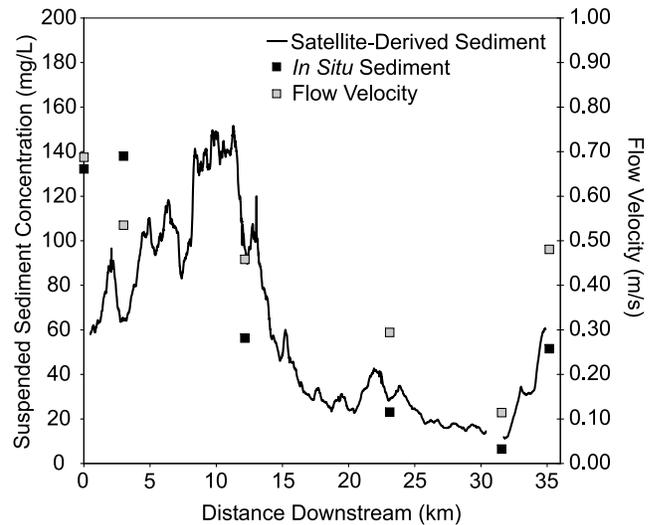
appropriate regression relationship between velocity and reflectance remains uncertain (Figure 10) and may vary with time, complicating application of the method across dates and locations. Finally, for all of the methods presented here, in situ measurements are required to construct the
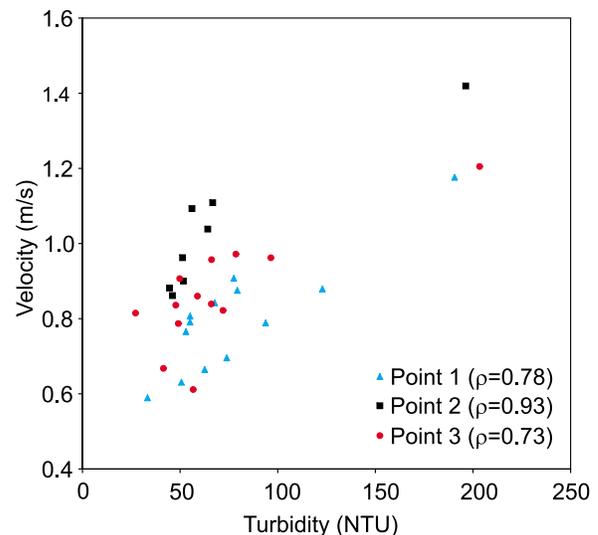

Figure 13. Scatterplot of relationships between velocity and turbidity for three points on the Athabasca River shown in Figure 1. Turbidity is used in place of SSC because of greater available sample size. Positive values of Spearman's ρ in all three cases (statistically significant at $p < 0.05$) suggest that it may be possible to remotely monitor variations in velocity over time by exploiting the velocity-SSC relationship.

requisite empirical relationships between satellite-derived reflectance, suspended solids, and hydraulic variables.

References

Alsdorf, D. E. (2003), Water storage of the central Amazon floodplain measured with GIS and remote sensing imagery, *Ann. Assoc. Am. Geogr.*, 93(1), 55–66, doi:10.1111/1467-8306.93105.

Alsdorf, D. E., and D. P. Lettenmaier (2003), Tracking fresh water from space, *Science*, 301, 1491–1494, doi:10.1126/science.1089802.

Alsdorf, D. E., J. M. Melack, T. Dunne, L. A. K. Mertes, L. L. Hess, and L. C. Smith (2000), Interferometric radar measurements of water level changes on the Amazon flood plain, *Nature*, 404(6774), 174–177, doi:10.1038/35004560.

Alsdorf, D. E., E. Rodriguez, and D. P. Lettenmaier (2007a), Measuring surface water from space, *Rev. Geophys.*, 45, RG2002, doi:10.1029/2006RG000197.

Alsdorf, D. E., P. Bates, J. Melack, M. Wilson, and T. Dunne (2007b), Spatial and temporal complexity of the Amazon flood measured from space, *Geophys. Res. Lett.*, 34, L08402, doi:10.1029/2007GL029447.

Aranuvachapun, S., and D. E. Walling (1988), Landsat-MSS radiance as a measure of suspended sediment in the lower Yellow River (Hwang Ho), *Remote Sens. Environ.*, 25, 145–165, doi:10.1016/0034-4257(88)90098-3.

Ashmore, P., and E. Sauks (2006), Prediction of discharge from water surface width in a braided river with implications for at-a-station hydraulic geometry, *Water Resour. Res.*, 42, W03406, doi:10.1029/2005WR003993.

Beltaos, S., T. D. Prowse, and T. Carter (2006), Ice regime of the lower Peace River and ice-jam flooding of the Peace-Athabasca Delta, *Hydrol. Processes*, 20(19), 4009–4029, doi:10.1002/hyp.6417.

Bjerklie, D. M., D. Moller, L. C. Smith, and S. L. Dingman (2005), Estimating discharge in rivers using remotely sensed hydraulic information, *J. Hydrol.*, 309, 191–209, doi:10.1016/j.jhydrol.2004.11.022.

Brakenridge, G. R., S. V. Nghiem, E. Anderson, and S. Chien (2005), Space-based measurement of river runoff, *Eos Trans. AGU*, 86(19), doi:10.1029/2005EO190001.

Brakenridge, G. R., S. V. Nghiem, E. Anderson, and R. Mic (2007), Orbital microwave measurement of river discharge and ice status, *Water Resour. Res.*, 43, W04405, doi:10.1029/2006WR005238.

Breusch, T. S., and A. R. Pagan (1979), A simple test for heteroscedasticity and random coefficient variation, *Econometrica*, 47, 1287–1294, doi:10.2307/1911963.

Chen, Z., P. J. Curran, and J. D. Hansom (1992), Derivative reflectance spectroscopy to estimate suspended sediment concentration, *Remote Sens. Environ.*, 40, 67–77, doi:10.1016/0034-4257(92)90127-6.

Choubey, V. K. (1998), Laboratory experiment, field and remotely sensed data analysis for the assessment of suspended solids concentration and secchi depth of the reservoir surface water, *Int. J. Remote Sens.*, 19(17), 3349–3360, doi:10.1080/014311698214037.

Coe, M. T., and C. M. Birkett (2004), Calculation of river discharge and prediction of lake height from satellite radar altimetry: Example for the Lake Chad basin, *Water Resour. Res.*, 40, W10205, doi:10.1029/2003WR002543.

Cook, R. D. (1977), Detection of influential observations in linear regression, *Technometrics*, 19(1), 15–18, doi:10.2307/1268249.

Cozar, A., C. M. Garcia, J. A. Galvez, S. A. Loiselle, L. Bracchini, and A. Cognetta (2005), Remote sensing imagery analysis of the lacustrine system of Ibera wetland (Argentina), *Ecol. Modell.*, 186, 29–41, doi:10.1016/j.ecolmodel.2005.01.029.

Curran, P. J., and E. M. Novo (1988), The relationship between suspended sediment concentration and remotely sensed spectral radiance: A review, *J. Coastal Res.*, 4(8), 361–385.

Dekker, A. G., R. J. Vos, and S. W. Peters (2001), Comparison of remote sensing data, model results and in situ data for total suspended matter (TSM) in the southern Frisian lakes, *Sci. Total Environ.*, 268, 197–214, doi:10.1016/S0048-9697(00)00679-3.

Dekker, A. G., R. J. Vos, and S. W. Peters (2002), Analytical algorithms for lake water TSM estimation for retrospective analyses of TM and SPOT sensor data, *Int. J. Remote Sens.*, 23(1), 15–35, doi:10.1080/0143116010006917.

Doxaran, D., J. M. Froidefond, S. Lavender, and P. Castaing (2002), Spectral signature of highly turbid waters application with SPOT data to quantify suspended particulate matter concentrations, *Remote Sens. Environ.*, 81, 149–161, doi:10.1016/S0034-4257(01)00341-8.

Doxaran, D., J. M. Froidefond, and P. Castaing (2003), Remote-sensing reflectance of turbid sediment-dominated waters. Reduction of sediment type variations and changing illumination conditions effect by use of reflectance ratios, *Appl. Opt.*, 42(15), 2623–2634, doi:10.1364/AO.42.002623.

Ekercin, S. (2007), Water quality retrievals from high resolution Ikonos multispectral imagery: A case study in Istanbul, Turkey, *Water Air Soil Pollut.*, 183, 239–251, doi:10.1007/s11270-007-9373-5.

Frappart, F., S. Calmant, M. Cauhope, F. Seyler, and A. Cazenave (2006), Preliminary results of ENVISAT RA-2–derived water levels validation over the Amazon Basin, *Remote Sens. Environ.*, 100, 252–264, doi:10.1016/j.rse.2005.10.027.

Fraser, R. N. (1998), Multispectral remote sensing of turbidity among Nebraska Sand Hills lakes, *Int. J. Remote Sens.*, 19(15), 3011–3016, doi:10.1080/014311698214406.

Frazier, P., K. Page, J. Louis, S. Briggs, and A. I. Robertson (2003), Relating wetland inundation to river flow using Landsat TM data, *Int. J. Remote Sens.*, 24(19), 3755–3770, doi:10.1080/0143116021000023916.

Gomez, B., L. A. K. Mertes, J. D. Phillpe, F. J. Magilligan, and L. A. James (1995), Sediment characteristics of an extreme flood: 1993 upper Mississippi River valley, *Geology*, 23(11), 963–966, doi:10.1130/0091-7613(1995)023<0963:SCOAEF>2.3.CO;2.

Griffiths, M., A. Taylor, and D. Woynillowicz (2006), Troubled waters, troubling trends: Technology and policy options to reduce water use in oil and oil sands development in Alberta, report, Pembina Inst., Drayton Valley, Alberta, Canada.

Han, L. (1997), Spectral reflectance with varying suspended sediment concentrations in clear and algae-laden waters, *Photogramm. Eng. Remote Sens.*, 63(6), 701–705.

Han, L., and D. C. Rundquist (1996), Spectral characterization of suspended sediments generated from two texture classes of clay soil, *Int. J. Remote Sens.*, 17(3), 643–649, doi:10.1080/01431169608949034.

Han, Z., Y.-Q. Jin, and C.-X. Yun (2006), Suspended sediment concentrations in the Yangtze River estuary retrieved from the CMODIS data, *Int. J. Remote Sens.*, 27(19), 4329–4336, doi:10.1080/01431160600658164.

Hellweger, F. L., W. Miller, and K. S. Oshodi (2006), Mapping turbidity in the Charles River, Boston using a high resolution satellite, *Environ. Monit. Assess.*, 132, 311–320, doi:10.1007/s10661-006-9535-8.

Holyer, R. J. (1978), Toward universal multispectral suspended sediment algorithms, *Remote Sens. Environ.*, 7, 323–338, doi:10.1016/0034-4257(78)90023-8.

Islam, M. R., Y. Yamaguchi, and K. Ogawa (2001), Suspended sediment in the Ganges and Brahmaputra rivers in Bangladesh: Observation from TM and AVHRR data, *Hydrol. Processes*, 15, 493–509, doi:10.1002/hyp.165.

Justice, C. O., J. R. G. Townshend, E. F. Vermote, E. Masuoka, R. E. Wolfe, N. Saleous, D. P. Roy, and J. T. Morisette (2002), An overview of MODIS land data processing and product status, *Remote Sens. Environ.*, 83, 3–15, doi:10.1016/S0034-4257(02)00084-6.

Keiner, L. E., and X. H. Yah (1998), A neural network model for estimating sea surface chlorophyll and sediments from thematic mapper imagery, *Remote Sens. Environ.*, 66, 153–165, doi:10.1016/S0034-4257(98)00054-6.

Knighton, D. (1998), *Fluvial Forms and Processes: A New Perspective*, Arnold, London.

Kouraev, A. V., E. A. Zakharova, O. Samain, N. M. Mognard, and A. Cazenave (2004), Ob' river discharge from TOPEX/Poseidon satellite altimetry (1992–2002), *Remote Sens. Environ.*, 93, 238–245, doi:10.1016/j.rse.2004.07.007.

Lathrop, R. G. (1992), Landsat Thematic Mapper monitoring of turbid inland water quality, *Photogramm. Eng. Remote Sens.*, 58(4), 465–470.

Lathrop, R. G., T. M. Lillesand, and B. S. Yandell (1991), Testing the utility of simple multi-date Thematic Mapper calibration algorithms for monitoring turbid inland waters, *Int. J. Remote Sens.*, 12(10), 2045–2063, doi:10.1080/01431169108955235.

Leconte, R., A. Pietroniro, D. L. Peters, and T. D. Prowse (2001), Effects of flow regulation on hydrologic patterns of a large, inland delta, *Reg. Rivers Res. Manage.*, 17, 51–65, doi:10.1002/1099-1646(200101/02)17:1<51::AID-RRR588>3.0.CO;2-V.

Leopold, L. B., and T. Maddock (1953), The hydraulic geometry of stream channels and some physiographic implications, *U.S. Geological Survey Prof. Pap.*, 252, 57 pp.

Liedeke, J., A. Roberts, and J. Luternauer (1995), Practical remote sensing of suspended sediment concentration, *Photogramm. Eng. Remote Sens.*, *61*(2), 167–175.

Liu, Y., M. A. Islam, and J. Gao (2003), Quantification of shallow water quality parameters by means of remote sensing, *Prog. Phys. Geogr.*, *27*(1), 24–43, doi:10.1191/0309133303pp357ra.

Maidment, D. R. (Ed.) (1993), *Handbook of Hydrology*, 1242 pp., McGraw-Hill, New York.

Matsuhisa, T., and C. Fukushima (2008), Methods for retrieving hydrologically significant surface parameters from remote sensing: A review for applications to East Asia region, *Hydrol. Processes*, *23*, 524–533.

McPherson, G. (2001), *Applying and Interpreting Statistics: A Comprehensive Guide*, 640 pp., Springer, New York.

Mertes, L. A. K. (2000), Inundation hydrology, in *Inland Flood Hazards: Human, Riparian, and Aquatic Communities*, edited by E. E. Wohl, pp. 145–166, Cambridge Univ. Press, New York.

Mertes, L. A. K. (2002), Remote sensing of riverine landscapes, *Freshwater Biol.*, *47*, 799–816, doi:10.1046/j.1365-2427.2002.00909.x.

Mertes, L. A. K., M. O. Smith, and J. B. Adams (1993), Estimating suspended sediment concentrations in surface waters of the Amazon River wetlands from Landsat images, *Remote Sens. Environ.*, *43*, 281–301, doi:10.1016/0034-4257(93)90071-5.

Miller, R. L., and B. A. McKee (2004), Using MODIS Terra 250 m imagery to map concentrations of total suspended matter in coastal waters, *Remote Sens. Environ.*, *93*, 259–266, doi:10.1016/j.rse.2004.07.012.

Nellis, M. D., J. A. Harrington, and J. Wu (1998), Remote sensing of temporal and spatial variations in pool size, suspended sediment, turbidity, and Secchi depth in Tuttle Creek Reservoir, Kansas: 1993, *Geomorphology*, *21*, 281–293, doi:10.1016/S0169-555X(97)00067-6.

Novo, E. M. M., J. D. Hansom, and P. J. Curran (1989), 'The effect of sediment type on the relationship between reflectance and suspended sediment concentration, *Int. J. Remote Sens.*, *10*(7), 1283–1289, doi:10.1080/01431168908903967.

Novo, E. M. M., C. A. Steffen, and C. Z. Bruga (1991), Results of a laboratory experiment relating spectral reflectance with total suspended solids, *Remote Sens. Environ.*, *36*, 67–72, doi:10.1016/0034-4257(91)90031-Z.

Peace-Athabasca Delta Project Group (1973), Technical report: A report on low water levels in Lake Athabasca and their effect on the Peace-Athabasca Delta, 176 pp., Ottawa, Canada.

Pavelsky, T. M., and L. C. Smith (2008a), Remote sensing of hydrologic recharge in the Peace-Athabasca Delta, Canada, *Geophys. Res. Lett.*, *35*, L08403, doi:10.1029/2008GL033268.

Pavelsky, T. M., and L. C. Smith (2008b), Rivwidth: A software tool for the calculation of river widths from remotely sensed imagery, *IEEE Geosci. Remote Sens. Lett.*, *5*(1), 70–73, doi:10.1109/LGRS.2007.908305.

Pavelsky, T. M., and L. C. Smith (2009), Surface water elevation and quality, Peace-Athabasca Delta, Canada, 2006–2007, http://daac.ornl.gov, Oak Ridge Natl. Lab. Distrib. Activ. Arch. Cent., Oak Ridge, Tenn., doi:10.3334/ORNLDAAC/935

Peters, D. L., T. D. Prowse, A. Pietroniro, and R. Leconte (2006), Flood hydrology of the Peace-Athabasca Delta, northern Canada, *Hydrol. Processes*, *20*, 4073–4096, doi:10.1002/hyp.6420.

Pietroniro, A., T. D. Prowse, and D. L. Peters (1999), Hydrologic assessment of an inland freshwater delta using multi-temporal satellite remote sensing, *Hydrol. Processes*, *13*, 2483–2498, doi:10.1002/(SICI)1099-1085(199911)13:16<2483::AID-HYP934>3.0.CO;2-9.

Pinkerton, M. H., K. M. Richardson, P. W. Boyd, M. P. Gall, J. Zeldis, M. D. Oliver, and R. J. Murphy (2005), Intercomparison of ocean colour band-ratio algorithms for chlorophyll concentrations in the subtropical front east of New Zealand, *Remote Sens. Environ.*, *97*, 382–402.

Prowse, T. D., and F. M. Conly (2002), A review of hydroecological results of the Northern River Basins Study, Canada. Part 2. Peace-Athabasca Delta, *River Res. Appl.*, *18*, 447–460, doi:10.1002/rra.682.

Prowse, T. D., and V. Lalonde (1996), Open-water and ice-jam flooding of a northern delta, *Nordic Hydrol.*, *27*, 85–100.

Quibell, G. (1991), The effect of suspended sediment on reflectance from freshwater algae, *Int. J. Remote Sens.*, *12*(1), 177–182, doi:10.1080/01431169108929642.

Raclot, D. (2006), Remote sensing of water levels on floodplains: A spatial approach guided by hydraulic functioning, *Int. J. Remote Sens.*, *27*(12), 2553–2574, doi:10.1080/01431160600554397.

Ritchie, J. C., and C. M. Cooper (1988), Comparison of measured suspended sediment concentrations with suspended sediment concentrations estimated from Landsat MSS data, *Int. J. Remote Sens.*, *9*(3), 379–387, doi:10.1080/01431168808954861.

Ritchie, J. C., and C. M. Cooper (1991), An algorithm for estimating surface suspended sediment concentrations with Landsat MSS digital data, *Water Resour. Bull.*, *27*(3), 373–379.

Ritchie, J. C., F. R. Schiebe, and J. R. McHenry (1976), Remote sensing of suspended sediments in surface waters, *Photogramm. Eng. Remote Sens.*, *42*, 1539–1545.

Ritchie, J. C., P. V. Zimba, and J. H. Everitt (2003), Remote sensing techniques to assess water quality, *Photogramm. Eng. Remote Sens.*, *69*(6), 695–704.

Ruhl, C. A., D. H. Shoellhamer, R. P. Stumpf, and C. L. Lindsay (2001), Combined use of remote sensing and continuous monitoring to analyze the variability of suspended-sediment concentrations in San Francisco Bay, California, *Estuarine Coastal Shelf Sci.*, *53*, 801–812, doi:10.1006/ecss.2000.0730.

Schiebe, F. R., J. A. Harrington Jr., and J. C. Ritchie (1992), Remote sensing of suspended sediments: The Lake Chicot, Arkansas project, *Int. J. Remote Sens.*, *13*(8), 1487–1509, doi:10.1080/01431169208904204.

Schindler, D. W., and W. F. Donahue (2006), An impending water crisis in Canada's western prairie provinces, *Proc. Natl. Acad. Sci. U. S. A.*, *103*(19), 7210–7216, doi:10.1073/pnas.0601568103.

Schmugge, T. J., W. P. Kustas, J. C. Ritchie, T. J. Jackson, and A. Rango (2002), Remote sensing in hydrology, *Adv. Water Resour.*, *25*, 1367–1385, doi:10.1016/S0309-1708(02)00065-9.

Shi, W., and M. Wang (2009), Satellite observations of flood-driven Mississippi River plume in the spring of 2008, *Geophys. Res. Lett.*, *36*, L07607, doi:10.1029/2009GL037210.

Siegmund, R., M. Bao, S. Lehner, and R. Mayerle (2004), First demonstration of surface currents imaged by hybrid along- and cross-track interferometric SAR, *IEEE Trans. Geosci. Remote Sens.*, *42*(3), 511–519, doi:10.1109/TGRS.2003.817816.

Smith, D. L. (1994), Glacial Lake McConnell: Paleogeography, age, duration, and associated river deltas, Mackenzie River Basin, western Canada, *Quat. Sci. Rev.*, *13*, 829–843, doi:10.1016/0277-3791(94)90004-3.

Smith, L. C. (1997), Satellite remote sensing of river inundation area, stage, and discharge: A review, *Hydrol. Processes*, *11*, 1427–1439, doi:10.1002/(SICI)1099-1085(199708)11:10<1427::AID-HYP473>3.0.CO;2-S.

Smith, L. C., and D. E. Alsdorf (1998), Control on sediment and organic carbon delivery to the Arctic Ocean revealed with spaceborne synthetic aperture radar: Ob' River, Siberia, *Geology*, *26*(5), 395–398, doi:10.1130/0091-7613(1998)026<0395:COSAOC>2.3.CO;2.

Smith, L. C., and T. M. Pavelsky (2008), Estimation of river discharge, propagation speed, and hydraulic geometry from space: Lena River, Siberia, *Water Resour. Res.*, *44*, W03427, doi:10.1029/2007WR006133.

Smith, L. C., and T. M. Pavelsky (2009), Remote sensing of volumetric storage change in lakes, *Earth Surf. Processes Landforms*, *34*(10), 1353–1358, doi:10.1002/esp.1822.

Smith, L. C., B. L. Isacks, R. R. Forster, A. L. Bloom, and I. Preuss (1995), Estimation of discharge from braided glacial rivers using ERS-1 synthetic aperture: First results, *Water Resour. Res.*, *31*(5), 1325–1329, doi:10.1029/95WR00145.

Smith, L. C., B. L. Isacks, A. L. Bloom, and A. B. Murray (1996), Estimation of discharge from three braided rivers using synthetic aperture radar (SAR) satellite imagery: Potential applications to ungaged basins, *Water Resour. Res.*, *32*(7), 2021–2034, doi:10.1029/96WR00752.

Spearman, C. (1904), The proof and measurement of association between two things, *Am. J. Psychol.*, *15*, 72–101.

Sterckx, S., E. Knaeps, M. Bollen, K. Trouw, and R. Houthuys (2007), Retrieval of suspended sediment from advanced hyperspectral sensor data in the Scheldt Estuary at different stages in the tidal cycle, *Mar. Geod.*, *30*(1), 97–108, doi:10.1080/01490410701296341.

Stumpf, R. P., and J. R. Pennock (1989), Calibration of a general optical equation for remote sensing of suspended sediments in a moderately turbid estuary, *J. Geophys. Res.*, *94*(C10), 14,363–14,371, doi:10.1029/JC094iC10p14363.

Tassan, S. (1994), Local algorithms using SeaWiFS data for the retrieval of phytoplankton, pigments, suspended sediment, and yellow substance in coastal waters, *Appl. Opt.*, *33*(12), 2369–2378, doi:10.1364/AO.33.002369.

Tassan, S. (1997), A numerical model for the detection of sediment concentration in stratified river plumes using Thematic Mapper data, *Int. J. Remote Sens.*, *18*(12), 2699–2705, doi:10.1080/014311697217567.

Temimi, M., R. Leconte, F. Brissette, and N. Chaouch (2005), Flood monitoring over the Mackenzie River Basin using passive microwave data, *Remote Sens. Environ.*, *98*, 344–355.

Teodoro, A. C., H. Goncalves, F. Veloso-Gomes, and J. A. Goncalves (2008), Modeling of the Douro River Plume size, obtained through im-

age segmentation of MERIS data, *IEEE Geosci. Remote Sens. Lett.*, *6*(1), 87–91, doi:10.1109/LGRS.2008.2008446.

Timoney, K. (2006), Landscape cover change in the Peace-Athabasca Delta, 1927–2001, *Wetlands*, *26*(3), 765–778, doi:10.1672/0277-5212(2006)26[765:LCCITP]2.0.CO;2.

Timoney, K. (2009), Three centuries of change in the Peace-Athabasca Delta, Canada, *Clim. Change*, *93*, 485–515, doi:10.1007/s10584-008-9536-4.

Tolk, B. L., L. Han, and D. C. Rundquist (2000), The impact of bottom brightness on spectral reflectance of suspended sediments, *Int. J. Remote Sens.*, *21*(11), 2259–2268, doi:10.1080/01431160050029558.

Topliss, B. J., C. L. Almos, and P. R. Hill (1990), Algorithms for remote sensing of high concentration, inorganic suspended sediment, *Int. J. Remote Sens.*, *11*(6), 947–966, doi:10.1080/01431169008955069.

Townsend, P. A., and J. R. Foster (2002), A synthetic aperture radar-based model to assess historical changes in lowland floodplain hydroperiod, *Water Resour. Res.*, *38*(7), 1115, doi:10.1029/2001WR001046.

Toyra, J., and A. Pietroniro (2005), Towards operational monitoring of a northern wetland using geomatics-based techniques, *Remote Sens. Environ.*, *97*, 174–191, doi:10.1016/j.rse.2005.03.012.

Tripathi, N. K., C. Venkobachar, R. K. Singh, and S. P. Singh (1998), Monitoring the pollution of river Ganga by tanneries using the multiband ground truth radiometer, ISPRS, *J. Photogramm. Remote Sens.*, *53*, 204–216, doi:10.1016/S0924-2716(98)00008-2.

Wang, F., B. Zhou, J. Xu, L. Song, and X. Wang (2008), Application of neural network and MODIS 250 m imagery for estimating suspended sediments concentration in Hangzhou Bay, China, *Environ. Geol.*, *56*, 1093–1101, doi:10.1007/s00254-008-1209-0.

Wass, P. D., S. D. Marks, J. W. Finch, G. J. Leeks, and J. K. Ingram (1997), Monitoring and preliminary interpretation of in-river turbidity and remote sensed imagery for suspended sediment transport studies in the Humber catchment, *Sci. Total Environ.*, *194–195*, 263–283, doi:10.1016/S0048-9697(96)05370-3.

Wolfe, B. B., T. L. Karst-Riddoch, S. R. Vardy, M. D. Falcone, R. I. Hall, and T. W. D. Edwards (2005), Impacts of climate and river flooding on the hydro-ecology of a floodplain basin, Peace-Athabasca Delta, Canada since AD 1700, *Quat. Res.*, *64*(2), 147–162, doi:10.1016/j.yqres.2005.05.001.

Wolfe, B. B., T. L. Karst-Riddoch, R. I. Hall, T. W. Edwards, M. C. English, R. Palmini, S. McGowan, P. R. Leavitt, and S. R. Vardy (2007), Classification of hydrologic regimes of northern floodplain basins (Peace-Athabasca Delta, Canada) from analysis of stable isotopes and water chemistry, *Hydrol. Processes*, *21*, 151–168, doi:10.1002/hyp.6229.

Woodruff, D. L., R. P. Stumpf, J. A. Scope, and H. W. Paerl (1999), Remote estimation of water clarity in optically complex estuarine waters, *Remote Sens. Environ.*, *68*, 41–52, doi:10.1016/S0034-4257(98)00108-4.

Wren, D. G., B. D. Barkdoll, R. A. Kuhnle, and R. W. Derrow (2000), Field techniques for suspended sediment measurement, *J. Hydraul. Eng.*, *126*(2), 97–104, doi:10.1061/(ASCE)0733-9429(2000)126:2(97).

Wu, G., J. Leeuw, A. K. Skidmore, H. H. Prins, and Y. Liu (2007), Concurrent monitoring of vessels and water turbidity enhances the strength of evidence in remotely sensed dredging impact assessment, *Water Res.*, *41*, 3271–3280, doi:10.1016/j.watres.2007.05.018.

Xia, L. (1993), A united model for quantitative remote sensing of suspended sediment concentration, *Int. J. Remote Sens.*, *14*(14), 2665–2676, doi:10.1080/01431169308904300.

———————————

T. M. Pavelsky, Department of Geological Sciences, University of North Carolina at Chapel Hill, Chapel Hill, NC 27599, USA. (pavelsky@unc.edu)

L. C. Smith, Department of Geography, University of California, Los Angeles, CA 90095, USA.